ChemElectroChem

Research Article
doi.org/10.1002/celc.202400712

Chemistry Europe
European Chemical Societies Publishing

www.chemelectrochem.org

The Oxidized $Ti_2(Al/Sn)C$ Behavior as Anode for Lithium- and Sodium-Ion Batteries: The Role of the MAX Phase Order

Nicholas Vallana, Irene Ostroman, Stefano Marchionna, Carla Palladini, Antonio Gentile, Omar Perego, Denis Sheptyakov, Andrew Fitch, Chiara Ferrara,* and Riccardo Ruffo

In the recent framework of the studies of Sn-doped MAX phase materials for potential applications as negative electrode materials in alkaline-ion batteries, this work explores the potentiality of the pure 211 MAX phase $Ti_2Al_{(1-y)}Sn_y$ compound through solid-state synthesis and subsequent thermal oxidation. A complete structural investigation through neutron diffraction and thermal operando synchrotron X-ray diffraction elucidates the phase evolution during oxidation. In coin cell tests against lithium, both samples demonstrate initial anodic capacities attributed to irreversible conversion reactions, followed by reversible alloying/dealloying mechanisms. Similarly, tests against sodium show comparable electrochemical behavior, albeit with lower capacities due to sodium's lower reactivity with Sn oxide. The capacity retention after cycling can be associated to the structural stability of the electrodes. Overall, this study has a place in the broader framework of the Sn-doped MAX phases investigation, and once more it underscores the importance of optimizing Sn oxide formation for enhanced electrochemical performance in both Li-ion and Na-ion batteries, with implications for future active materials design.

1. Introduction

The urgent necessity to address the environmental repercussions of fossil fuels continues to propel research endeavors in the domain of energy storage. Various technologies rely heavily on batteries that are safe, offer high performance, and are cost-effective. Lithium-ion batteries (LIBs) have emerged as the predominant energy storage technology owing to their reliability and good electrochemical storage capabilities.[1]

However, the downsides linked with graphite, the most used negative electrode in LIBs, such as unsafe usage at elevated currents and aging concerns, persist in propelling research toward materials capable of delivering superior performance. Moreover, in general, the large-scale production of LIBs faces a significant challenge due to constraints in the availability of raw materials, with lithium itself being particularly scarce relative to the projected future need for batteries.[2]

Other alkaline ion batteries have been studied extensively, and replacing lithium with sodium has emerged as a promising alternative.[3–6] Sodium-ion batteries (SIBs) exhibit a similar mechanism to LIBs. However, the negative electrode is critical in SIBs since graphite is unsuitable due to sodium's inability to intercalate into it.[7,8]

Conversion/alloying oxides (SnO_2, SiO_x) are a class of negative electrode materials that have been widely studied due to their high specific capacity,[9–13] but generally are not practical due to the mechanical instability of the electrodes. A possible solution is the use of composite materials in which a buffer system is able to mitigate the volumetric expansions due to electrode pulverization.[14–18] Moreover, several studies indicate that the long-term stability of SnO_2 can be improved in both LIBs[19–23] and SIBs[21] when combined with other metal oxides, particularly TiO_2, in the form of mixed-oxide composites. In this context, metallic MAX phases are of particular interest as precursors for nanocomposites. Sn or Si containing MAX phases are ideal platforms for the preparation of composites, provided that a certain amount of MAX is present after the treatment. In fact, MAX has metallic conductivity (of the order of 3×10^6 S m^{-1}) and the formation of oxide nanoparticles occurs spontaneously on the surface during heat treatment, without the use of complex chemical reactions as in the case of MXene-based composites. Using this

N. Vallana, I. Ostroman, C. Palladini, C. Ferrara, R. Ruffo
Department of Materials Science
University of Milano Bicocca
Via Cozzi 55, 20125 Milano, Italy
E-mail: chiara.ferrara@unimib.it

S. Marchionna, A. Gentile, O. Perego
Ricerca sul Sistema Energetico
S.p.A.
Via R. Rubattino 54, 20134 Milano, Italy

D. Sheptyakov
Laboratory for Neutron Scattering and Imaging
Forschungstrasse 111, 5232 Villigen, Switzerland

A. Fitch
ID22, Structure of Materials Group
ESRF - The European Synchrotron
CS40220, F-38043, Cedex 9 Grenoble, France

C. Ferrara, R. Ruffo
GISEL-INSTM
Via G. Giusti 9, 50121 Firenze, Italy

Supporting information for this article is available on the WWW under https://doi.org/10.1002/celc.202400712

approach, the Ti_3AlC_2 312 MAX phase was recently synthesized in our group with a variable amount of Sn substituting Al in the MAX matrix and thermally oxidized, then it was directly used as anodic material in both LIBs[24] and SIBs.[24–26] This procedure leads to the formation of nanocomposite oxide compounds that show a high efficiency as negative electrodes.

For this work, a slightly different material has been employed: instead of synthesizing the 312 phase, we aimed to explore the 211 compounds, whose formula as doped phase is expressed as $Ti_2Al_{(1-x)}Sn_xC$, where X equals to 0.31 (sample Sn-low_RT) and 0.49 (sample Sn-high_RT). The use of phase 211 instead of 321 would have inherent advantages. In fact, in addition to similar or slightly higher metallic conductivity,[27] the 211 phase has a lower molar mass, which should result in higher specific capacity for the same MAX/oxide molar ratio since the MAX is almost inert in the electrochemical reaction. The materials were obtained via SPS synthesis and were oxidized through a thermal treatment at 700 °C (Sn-low_Ox and Sn-high_Ox).

Both pristine and oxidized samples have been extensively analyzed: the structure was retrieved by neutron diffraction (ND) and the structural change upon heating was studied by Operando Synchrotron X-ray diffraction (SXRD), confirmed by the results of transmission electron microscopy (TEM) investigation, while their thermal behavior was monitored by thermal gravimetric analysis (TGA), and the morphology was checked through scanning electron microscopy (SEM) and TEM. The materials were employed as negative electrode active materials for both lithium and sodium coin half cells through galvanostatic cycling with potential limitation (GCPL) rate test. These analyses and testing versus Li and Na allowed us for a critical comparison of the 312 and 211 classes of compounds and to rationalize the effect of the MAX phase order on the electrochemical performance when considered as anode material.

2. Results and Discussion

The Sn-low_RT and Sn-high_RT samples have been successfully prepared according to the experimental procedure reported in the Supporting Information. Both the samples are constituted by the desired 211 phase (ICSD code 98-060-4361), as evidenced from the neutron diffraction patterns reported in **Figure 1** and confirmed by the results of Rietveld refinements conducted on this data and reported in Figure S1 and Table S1, Supporting Information. A small fraction of 312 MAX phase is detected together with TiC, for both the samples; these represent the most common impurities reported in the production of MAX phases.[24] The presence of small amount of 312 phase is not detrimental for the final application. The variation of the cell parameters, reported in Table S1, Supporting Information, indicates an effective Sn substitution on the Al sites, confirming the successful preparation of the desired compositions. Indeed, with the increasing content of Sn both *a* and *c* parameters undergo an expansion and so does the volume. This effect can be correlated to the atomic radius and it is in line with previous reports on the 211 and 312 Sn-doped phases.[24,28–31]

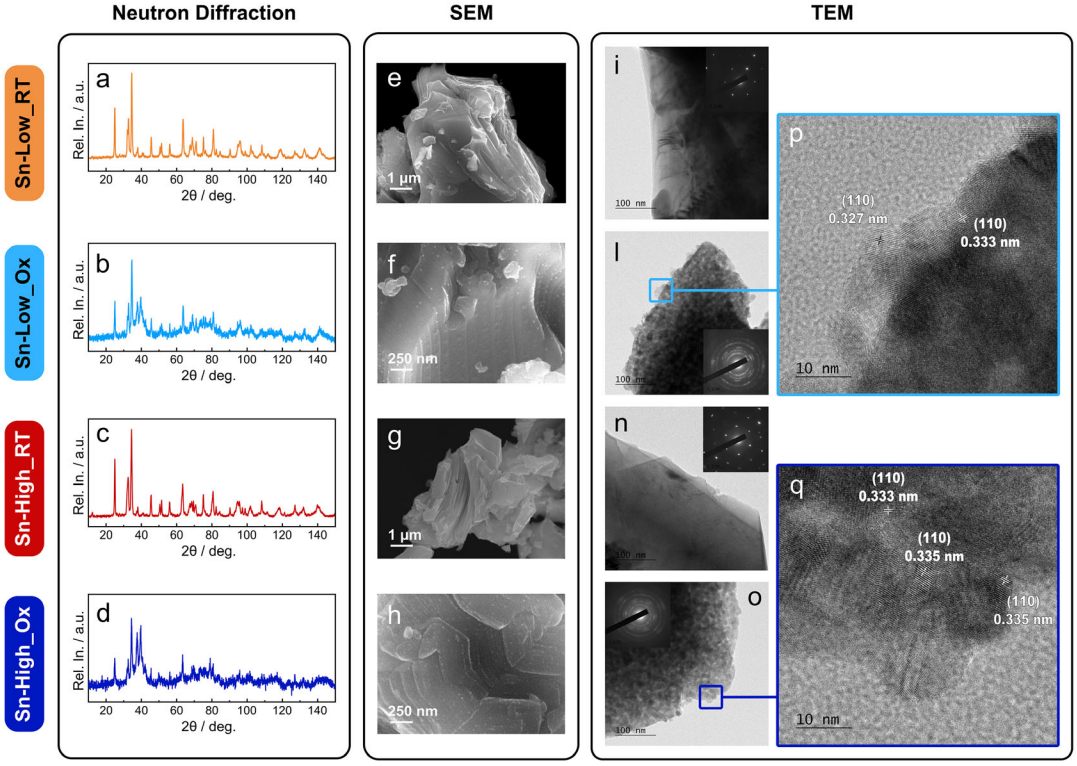

Figure 1. Neutron diffraction data, SEM, and TEM images of the samples Sn-low at RT a,e,i), Sn-low oxidized b,f,l), Sn-high at RT c,g,n), and Sn-High oxidized d,h,o). The insets of TEM images (i,l,n,o) are referred to the respective diffraction patterns; HRTEM images of Sn-low_Ox and Sn-high_Ox are reported in panels p) and q).

The structure is composed of Ti–C slabs spaced by Al/Sn layers, with Al and Sn sharing the same crystallographic sites. The Al/Sn ratio has been refined with the analysis of the neutron and synchrotron powder patterns; the results suggest that the Sn-low_RT samples correspond to the $Ti_2Al_{0.62}Sn_{0.38}C$ composition while the Sn-high_RT corresponds to the $Ti_2Al_{0.40}Sn_{0.60}C$ stoichiometry. Attempts to go through the highest Sn content led to the formation of higher amount of secondary phases suggesting that, possibly, the solubility limit of the Sn into the 211 has been reached with the Sn-high_RT sample. These two samples will be thus considered representative of low and high doping levels to rationalize the effect on the oxidizing behavior and, in turn, on the electrochemical properties of the oxidized samples. The morphology of the Sn-low_RT and Sn-high_RT evidence the layered structure of the system. Primary particles appear as compact lamellae with dimensions in the 5–10 μm size range with a wide distribution and elongated shape. To further support the results obtained from XRD investigation, TEM images have been collected for all the pristine and oxidized samples, as reported in Figure 1. The pristine (RT) samples (Figure 1i,n) present the typical MAX phase compact lamellar morphology and high crystalline order as evidenced by the corresponding single crystal-like diffraction patterns, in good agreement with previous report and XRD analysis.[24,26] On the contrary, the particles of the oxidized samples (Figure 1l,o) exhibit a nanocomposite morphology, where nanocrystals in the order of 10–20 nm in diameter cover the MAX phase core, still visible with the compact lamellar structure. From the HRTEM images of the oxidized samples (Figure 1p,q) are evident that the majority of these nanocrystals present the TiO_2/SnO_2 structure, demonstrating the formation of a MAX/oxides nanocomposite. Moreover, as a distribution of (110) planes d-spacing is observed (Figure 1p,q), this further supports the hypothesis of formation of oxides with mixed $(Ti/Sn)O_2$ as the d spacing observed are in the range defined by the two end members TiO_2 (PDF card 00-034-0180) correspond to 0.325 nm and for the SnO_2 (PDF card 01-087-9075) correspond to 0.335 nm. Globally the Sn-low and Sn-high samples presented the expected Al/Sn mixed compositions and the oxidized materials are composed of MAX phase core covered by nano dispersed $(Ti/Sn)O_2$ oxides; these results are well in line with our previous findings on the 312 series of samples with variable Al/Sn content.[24,26]

As already discussed in the introduction, the key point for obtaining high-performance negative electrode materials is the formation of the nanocomposite constituted by an inner core of conductive MAX phase covered with nanostructured $(Ti/Sn)O_2$ oxides enabling the conversion reaction.[24–26] The oxidation procedure has been carefully optimized by coupled thermal analysis and in-situ diffraction investigation, enabling for accurate follow-up of the oxidation reaction; results are reported in **Figure 2**. The differential thermal analysis (DTA), profiles reveal

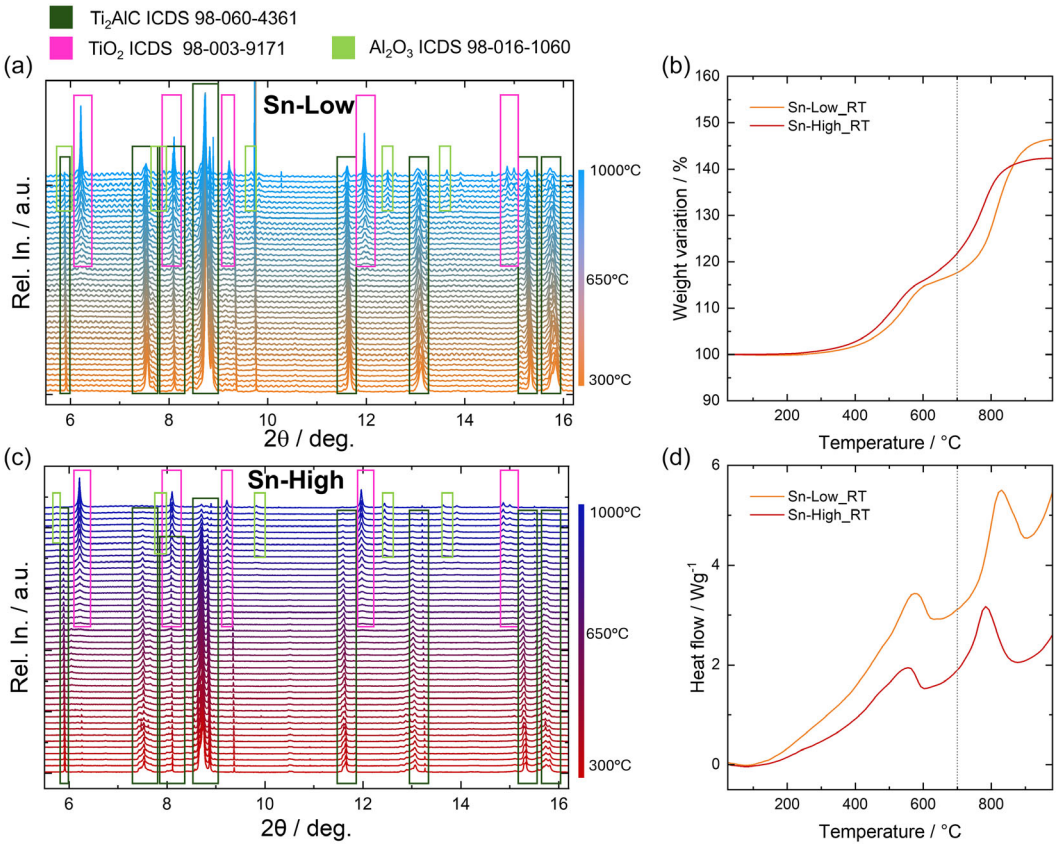

Figure 2. In-situ XRD data as a function of temperature in the 300–1000 °C a,c) and the thermal analysis and DTA profiles b,d) for the Sn-low_RT (a,c) and Sn-high_RT (b,d) samples. Frame in panels a and b indicates the phases: dark gray 211 reference phase ICDS 98-060-4361; pink rutile TiO_2 ICDS 98-003-9171; lime green corundum Al_2O_3 ICDS 98-016-1060.

for both samples two exothermic processes: the first at ≈600 °C and the second one at ≈800 °C; the onset temperature is affected by the composition of the sample, as evident from the TGA and DTA profiles in Figure 2c,d. The first peak has been associated with the oxidation of the MAX phase with the formation and crystallization of different oxides. This is confirmed by the analysis of the in-situ XRD data that show the appearance of very broad reflections corresponding to the formation of mixed (Ti/Sn)O_2 oxides (pink frames in Figure 2a,c, ICDS 98-003-9171), in good agreement with the observations from TEM analysis previously reported. At higher temperatures Al_2O_3 crystallizes (green frames in Figure 2a,c, ICDS 98-016-1060); this process can be associated with the second peak observed above 800 °C. Overall the 211 Ti_2(Al/Sn)C samples undergo almost complete conversion to the corresponding oxides at temperature above 1000 °C.

The global oxidation reaction can be thus written as

$$\mathrm{Ti_2Al_{(1-y)}Sn_yC} + x\left(\frac{15}{4}+\frac{y}{4}\right)\mathrm{O_2} \rightarrow (1-x)\mathrm{Ti_2Al_{(1-y)}Sn_yC} + 2x\mathrm{TiO_2} + yx\mathrm{SnO_2} + x\left(\frac{1-y}{2}\right)\mathrm{Al_2O_3} + x\mathrm{CO_2} \quad (1)$$

The effect of the Sn substitution is to lower the oxidation resistance of the 211 Al-based MAX phase, as already demonstrated by previous studies.[24,29,32–34] This is evident from the in-situ XRD at the highest temperature. Indeed, the XRD pattern of the Sn-low_RT samples at 1000 °C shows the reflection, even if decreased in intensity, of the initial 211 phase. On the contrary, the corresponding XRD pattern at 1000 °C for the Sn-high_RT sample shows strongly attenuated and broadened reflection of the 211, indicating that the oxidation of the initial material is almost completed. The different thermal resistance of the two samples is also evident by considering the TGA and DTA thermal profiles, very similar in shape but with a shift of ≈50 °C, for the MAX with higher Sn content.

As discussed in the introduction, the electrochemically active material is the MAX phase/oxides nanocomposite obtained through the oxidation of the pristine MAX phases. On the basis of the characterization of the thermal behavior and phase evolution of the pristine material, the preparation of the oxidized samples has been performed at 700 °C, enabling the initial oxidation of the MAX phase while avoiding the crystallization of Al_2O_3 on the surface of the lamellae. The effect of the thermal treatment on the morphology is revealed by the inspection of the SEM and TEM images reported in Figure 1. The appearance of smaller particles below in the range of 10–20 nm is evident, confirming that the selected thermal protocol allows controlling the oxidation in terms of obtained phases and morphology of the newly formed nanoparticles.

Based on this preliminary characterization, it is possible to rationalize the different electrochemical behavior of the two materials. The electrochemical properties of the samples as active material were studied in two-electrode coin half cells, first versus lithium, then versus sodium, focusing on rate test measures. The results concerning half cells versus lithium are summarized in **Figure 3**. In the Li-case, during the first cycle at low current

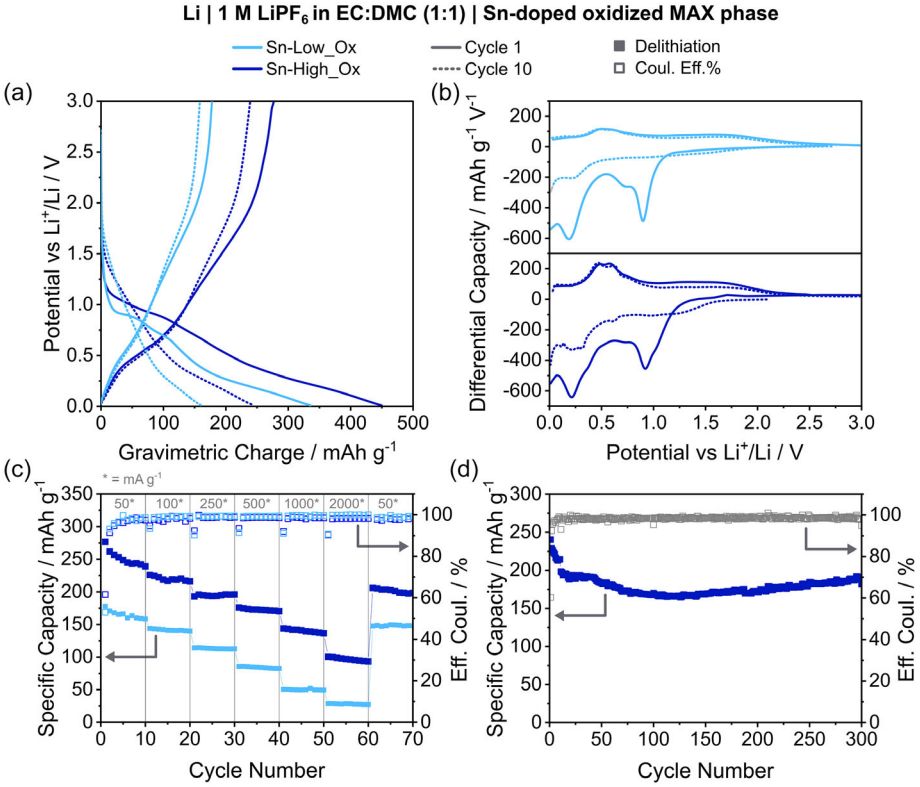

Figure 3. Electrochemical characterization of Sn-low_Ox and Sn-high_Ox in half cells versus lithium; a) potential profiles of cycles 1 and 10, b) differential capacity of cycles 1 and 10, c) rate test, and d) long cycling test.

(50 mA g^{-1}), the two Sn-low_Ox and Sn-high_Ox materials showed an anodic capacity of 177 and 277 mAh g^{-1} with a coulombic efficiency of 51% and 62%, respectively (Figure 3a). These efficiency values are related to the high irreversible nature of the conversion reaction of tin oxide: during the first lithiation, the tin oxide is reduced to metallic tin; then, at a lower potential, metallic tin goes through an alloying mechanism, forming a tin–lithium alloy.[12] The overall mechanism is the following

$$SnO_2 + 4Li^+ + 4e^- \rightarrow Sn + 2Li_2O \quad (2)$$

$$Sn + 4.4Li^+ + 4.4e^- \leftrightharpoons Li_{4.4}Sn \quad (3)$$

The alloying mechanism is a reversible process, while the conversion reactions have a partially irreversible nature. So, during the subsequent first delithiation, the reduced tin reoxidizes to metallic tin, but not completely to the starting tin oxide, leading to an anodic capacity lower than the respective cathodic capacity.[35] Concerning this, from the second cycle, the main reaction involved in the charge storage is the reversible alloying/dealloying mechanism, as confirmed by the rapid increase of the coulombic efficiency. After 10 cycles at low current, indeed, the Sn-low_Ox and Sn-high_Ox electrodes were able to deliver 160 and 240 mAh g^{-1} with efficiencies of 98.5%.

This behavior can be confirmed considering the differential capacity (Figure 3b). In particular, for the Sn-high_Ox, reduction peaks around 1.0 V and after 0.5 V are correlated to the conversion of tin oxide and the alloying reaction, respectively; instead, in the anodic part, oxidation peaks are visible only around 0.4–0.6 V, related to the reversible dealloying mechanism, while at higher potential is visible a broadening peak of the partially reconversion reaction that occurs.[36,37] On the contrary, for the Sn-low_Ox, the reduction peak occurs around 0.75 V and after 0.5 V: the absence of well-defined peaks around 1.0 V can be associated with the lower content of tin oxide that can react, compared to the Sn-high_Ox material, while the subsequent peak is associated to the SEI formation, less visible near the conversion peak in the Sn-high_Ox. During oxidation, a broadening peak around 0.5 V can be seen for the Sn-low_Ox, related to the reversible dealloying. Moreover, at cycle number 10, the first peak of cathodic conversion disappears, although the area subtended by the curve at potentials $>$1.0 V (both cathodic and anodic) is not zero, indicating that the conversion reaction may be partially reversible as also recently revealed by in situ analysis for the 312 analog compound.[37] The rate capability test, presented in Figure 3c allows for further comparison of the behavior of the two samples.

The presence of the high conductivity MAX phase is beneficial to the high rate performance of the electrode, as shown in the rate capability test performed on 70 cycles (Figure 3c) and changing the current after every 10 cycles (details can be found in the experimental part). Indeed, the Sn-high_Ox is still able to deliver reversible capacities of 215, 190, 175, 140, and 90 mAh g^{-1} at 0.10, 0.25, 0.50, 1.00, and 2.00 A g^{-1} current densities, respectively while significantly lower values are reported for the Sn-low_Ox (140, 115, 83, 48, 26 mAh g^{-1}, at the same current densities). The differences between the delivered capacities of the two samples can be related to the different amount of oxides (higher for the Sn-high, as highlighted by the TGA and in situ XRD analysis reported in Figure 2) and also for the higher tin content in the Sn-high samples. Indeed, as reported, tin is responsible for the reversible alloying reaction. At the higher currents, these electrodes are outperforming graphite which suffers of Li plating issues at these current densities. Due to the superior behavior of the Sn-high-Ox sample, long cycling test was finally performed, results are reported in Figure 3d. The results evidence that, after electrode stabilization at 50 mA g^{-1} the Sn-high_Ox electrode material is stable for 300 cycles at 100 mA g^{-1} in the half cell. The initial specific capacitance (average 15 cycles 225 ± 3 mAh g^{-1}) decreases to about 199 ± 1 mAh g^{-1} during the first 125 cycles and then increases again to 221 ± 2 mAh g^{-1} (last 10 cycles). This trend could be due to the cycling conditions performed at room temperature. Thus, the capacity retention is greater than 98% after 300 cycles.

For testing the properties of these materials versus the reaction with sodium ions, a similar analysis was carried out using half cells versus metallic sodium (**Figure 4**). During the first cycle, the two materials showed an anodic capacity of 65 and 109 mAh g^{-1} with a coulombic efficiency of 49% and 44%, respectively for Sn-low_Ox and Sn-high_Ox correlated to the irreversible conversion reaction, as for lithium (Figure 4a). Both materials require several cycle to stabilize the capacity and increase the charge efficiency. Indeed, at the cycle 10 the Sn-low_Ox and Sn-high_Ox electrodes delivered 61 and 78 mAh g^{-1} with charge efficiencies of 98%. This is probably due to the depth of the conversion reaction, which requires a few cycles to reduce all the SnO_2 present on the surface of the MAX. The reactions involved in the process are, indeed, analogous to the case of lithium:[13]

$$SnO_2 + 4Na^+ + 4e^- \rightarrow Sn + 2Na_2O \quad (4)$$

$$Sn + 3.75Na^+ + 3.75e^- \leftrightharpoons Na_{3.75}Sn \quad (5)$$

The cathodic peaks around 0.25 V are associated with the alloying of sodium with tin (Figure 4b), confirming the previous mechanism, with the corresponding peaks at the same value in the anodic scan related to the reversible dealloying process.[38] For the Sn-low_Ox sample, the anodic peak is less visible and broader due to the less amount of reacting tin, as seen with lithium. The conversion peaks are lost after the first cycle. The rate test was performed on 70 cycles, using lower values of current for both Sn-high and Sn-low oxidized samples: 15, 30, 75, 150, 750, 1500 e 15 mA g^{-1}. The sample Sn-high_Ox showed a mean capacity value of 80 mAh g^{-1} at a gravimetric current of 15 mA g^{-1}, which decreases to 50 mAh g^{-1} at 150 mA g^{-1} (Figure 4c) while Sn-low_Ox presents even lower mean capacity values of 60 and 30 mAh g^{-1} at 15 and 150 mA g^{-1}. The further increase of the current to 750 mA g^{-1} provokes a drastic decrease of the capacity (around 20 mAh g^{-1} for the Sn-high_Ox). Again the differences among the two samples dwell in the different oxide content and, within this, the different tin composition.

Also in this case, long cycling test has been performed only for the Sn-high_Ox composition and was conducted at 30 mA g^{-1} after the stabilization at 15 mA g^{-1}. The initial specific capacity is 74.4 ± 0.6 mAh g^{-1} at cycles 11–20 and remains stable for about

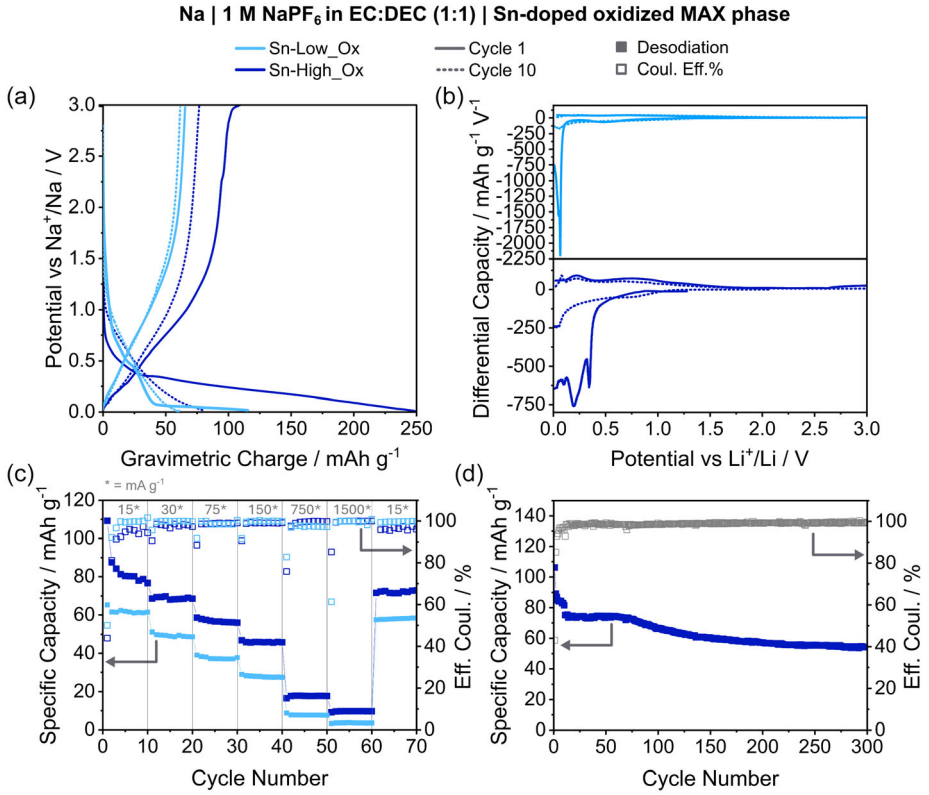

Figure 4. Electrochemical characterization of Sn-low_Ox and Sn-high_Ox in half cells versus sodium; a) potential profiles of cycles 1 and 10, b) differential capacity of cycles 1 and 10, c) rate test, and d) long cycling test.

60 cycles (Figure 4d). After that, it starts decreasing and reaches 54.3 ± 0.5 mAh g^{-1} at the end of the test with a capacity retention of 73%. Thus, despite similar reaction mechanisms, the performance of sodium is inferior to that of lithium in terms of both specific capacity and rate capability. This effect can be related to the higher volume variation that occurs when alloying/dealloying sodium, which affects the expected increase in capacity leading to worse performance.[37]

The results reported in the present work for the 211 oxidized MAX phases are a new notch in description of the oxidized MAX phases as possible anode materials for LIBs and SIBs applications. A comparison of the materials obtained under the same conditions (treatments at 700 °C) lead to different oxidation degrees. This in turns depend on two parameters: i) the MAX phase order; ii) the Sn content in the pristine MAX phase. To rationalize these two effects it is important to recall the oxidation reactions for the 211 and 312 differing only for the stoichiometry. The final goal is to optimize and tune the amount of residual MAX phase (beneficial for the stability) and the $(Ti/Sn)O_2$, (that have been demonstrated to be the electrochemically active species). This is particularly evident considering the results obtained for the electrochemical testing of the pristine 211 and 312 materials (Figure S2, Supporting Information), proving that the MAX phase alone provide only very limited capacity contribution.

Particularly Sn is the active component, undergoing sequential conversion and alloying reaction. Considering the same degree of oxidation (e.g., fixing the X value in Equation 1) it is easy to visualize that the higher the order of the MAX phase the higher is the amount of $(Ti/Sn)O_2$ oxide that can be produced. Moreover, the higher the tin content, the higher is the amount of tin in the final oxides. Thus high Sn contents are beneficial, as evident from results reported in Figure 3 and 4 for the 211 compositions and in our previous report for the 312 samples.[26] Regarding the effect of the MAX phases order, although it is true the high order (i.e., high Ti content due to the stoichiometry of the pristine 211 and 312 phases) brings to high %w of Ti-based oxide produced by the oxidation reaction, this is balanced by the weight to weight ratio of the residual MAX phase (lighter in the case of 211 respect to the 311 under the same degree of oxidation, i.e., fixing the $\times$ value in Equation 1).

The materials considered in this work are proposed as anodes in lithium and sodium batteries. In the first case, as discussed in the text, the reference material is graphite, compared to which the Sn_Ox_high sample has a lower specific capacity at low current (240 vs 370 mAh g^{-1}), but can be lithiated at extremely high currents (2 A g^{-1}, over 5C for graphite) with good performance (about 100 mAh g^{-1}, or about 40% SOC). Graphite cannot be lithiated at these currents. In terms of application in sodium batteries, the performance of these 211 phases is certainly not competitive with state-of-the-art materials, but they have good kinetic properties at high currents and could be of interest in pseudocapacitors. For a more detailed comparison of the properties of the oxidized MAX phase materials with other anode materials for SIBs, one can refer to our recent papers.[26,37] Globally this bottom-up approach for the controlled oxidation of materials fits in the emerging field on engineering of nano materials and

composites, of particular relevance for electrochemical energy storage applications.[39,40]

3. Conclusion

The 211 Sn-doped MAX phases have been successfully synthesized; the powder contains minor fraction of 312 phases and TiC, as demonstrated by the analysis of the neutron diffraction data and carefully characterized with respect to the phase evolution as a function of the temperature through in-situ XRD analysis and thermal analysis. The SEM and TEM characterization demonstrate the successful obtaining of a nanocomposite where the compact lamellar structure of the original MAX phase is preserved as a core while the surface of the MAX phase particles are covered with a dispersion of spherical $(Ti/Sn)O_2$ nanoparticles in the range of 10–20 nm. This characterization enabled us to define the optimal temperature for oxidizing treatment, which led to the production of the Sn-low_Ox and Sn-high-Ox samples to be considered for electrochemical testing versus Li and Na. The results show that obtaining a nanometric formation of SnO_2 is the key for good electrochemical performance, and its abundance is critical for higher storage capacity.

These results, summarized in **Figure 5**, can be rationalized by considering a wider frame, involving the evaluation of the 312 MAX phases tests versus Li and Na in our previous works.[24,26,39]

The capacity values are always higher for the 312 series with respect to the 211 phases, which is coherent with the fact that at 700 °C the amount of SnO_2 % in mass after the thermal oxidation is on average 27% for 312, while it is the 13% for 211 phase (see Table S2, Supporting Information for reference). This study also confirms an already observed trend in the previous works:[24,26] the increased content of Sn oxide has a more relevant impact on the specific capacity of the materials for lithium-ion half cells. Finally, it is also here confirmed that sodium has a worse reactivity with it. From a perspective, a deeper insight into the morphology-electrochemical properties is mandatory.

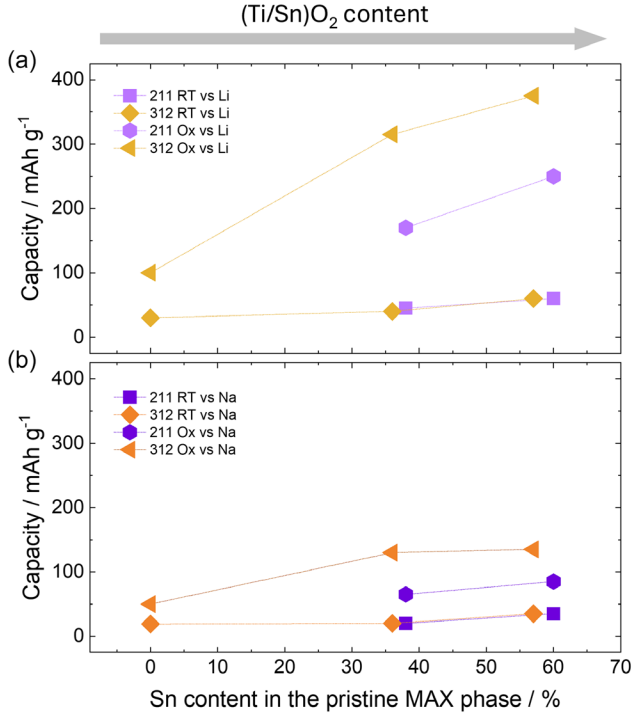

Figure 5. Capacity values for the 312 oxidized MAX phases[24,26,39] and 211 oxidized MAX phases (this work) as a function of the Sn content of the pristine MAX phases as determined from neutron diffraction analysis when testes versus Li a) and versuss Na b). All the MAX phases reported in this graph have been oxidized at 700 °C.

Acknowledgements

This work was realized thanks to the MOST - Sustainable Mobility Center and received funding from the European Union Next Generation EU (PIANO NAZIONALE DI RIPRESA E RESILIENZA (PNNR) Missione 4 Componente 2, Investimento 1.4 D.D. 1033 17/06/2022, CN00000023). This manuscript reflects only the authors' views and opinions, neither the European Union nor the European Commission can be considered responsible for them. This work has been financed by the Research Fund for the Italian Electrical System under the Three-Year Research Plan 2022–2024 (DM MITE n. 337, 15.09.2022), in compliance with the Decree of April 16th, 2018. This work is partially supported by the SMART-electron Project which has received funding from the European Union's Horizon 2020 Research and Innovation Programme under Grant Agreement No. 964591.

This work is partially based on experiments performed at the Swiss spallation neutron source SINQ, Paul Scherrer Institute, Villigen, Switzerland, and on experiment performed at the European Synchrotron Radiation Facility, Grenoble, France.

Conflict of Interest

The authors declare no conflict of interest.

Data Availability Statement

The data that support the findings of this study are available from the corresponding author upon reasonable request.

Keywords: alkaline-ion batteries · energy storage · MAX phase · nanocomposite · Sn oxide

[1] M. Armand, P. Axmann, D. Bresser, M. Copley, K. Edström, C. Ekberg, D. Guyomard, B. Lestriez, P. Novák, M. Petranikova, W. Porcher, S. Trabesinger, M. Wohlfahrt-Mehrens, H. Zhang, *J. Power Sources* **2020**, *479*, 228708.
[2] A. Amato, B. Alessandro, M. Villen-Guzman, C. Vereda Alonso, F. Beolchini, *J. Cleaner Prod.* **2021**, *300*, 126954.
[3] C. Delmas, *Adv. Energy Mater.* **2018**, *8*, 1703137.
[4] K. Chayambuka, G. Mulder, D. L. Danilov, P. H. L. Notten, *Adv. Energy Mater.* **2018**, *8*, 1800079.
[5] C. Vaalma, D. Buchholz, M. Weil, S. Passerini, *Nat. Rev. Mater.* **2018**, *3*, 1.
[6] P. K. Nayak, L. Yang, W. Brehm, P. Adelhelm, *Angew. Chem. Int. Ed.* **2018**, *57*, 102.
[7] D. A. Stevens, J. R. Dahn, *J. Electrochem. Soc.* **2001**, *148*, A803.

[8] Y. Li, Y. Lu, P. Adelhelm, M. M. Titirici, Y. S. Hu, *Chem. Soc. Rev.* **2019**, *48*, 4655.
[9] M. Shimizu, H. Usui, H. Sakaguchi, *J. Power Sources* **2014**, *248*, 378.
[10] J. M. Stratford, M. Mayo, P. K. Allan, O. Pecher, O. J. Borkiewicz, K. M. Wiaderek, K. W. Chapman, C. J. Pickard, A. J. Morris, C. P. Grey, *J. Am. Chem. Soc.* **2017**, *139*, 7273.
[11] W. T. Jing, C. C. Yang, Q. Jiang, *J. Mater. Chem. A* **2020**, *8*, 2913.
[12] M. Mirolo, X. Wu, C. A. F. Vaz, P. Novák, M. El Kazzi, *ACS Appl. Mater. Interfaces* **2021**, *13*, 2547.
[13] X. Wu, X. Lan, R. Hu, Y. Yao, Y. Yu, M. Zhu, *Adv. Mater.* **2022**, *34*, 2106895.
[14] J. W. Wang, X. H. Liu, S. X. Mao, J. Y. Huang, *Nano Lett.* **2012**, *12*, 5897.
[15] X. H. Liu, Y. Liu, A. Kushima, S. Zhang, T. Zhu, J. Li, J. Y. Huang, *Adv. Energy Mater.* **2012**, *2*, 722.
[16] M. Gu, A. Kushima, Y. Shao, J. G. Zhang, J. Liu, N. D. Browning, J. Li, C. Wang, *Nano Lett.* **2013**, *13*, 5203.
[17] J. Park, J. W. Park, J. H. Han, S. W. Lee, K. Y. Lee, H. S. Ryu, K. W. Kim, G. Wang, J. H. Ahn, H. J. Ahn, *Mater. Res. Bull.* **2014**, *58*, 186.
[18] T. Li, U. Gulzar, X. Bai, M. Lenocini, M. Prato, K. E. Aifantis, C. Capiglia, R. Proietti Zaccaria, *ACS Appl. Energy Mater.* **2019**, *2*, 860.
[19] R. Li, W. Xiao, C. Miao, R. Fang, Z. Wang, M. Zhang, *Ceram. Int.* **2019**, *45*, 13530.
[20] J. H. Um, J. Lim, K. Hengge, C. Scheu, W. S. Yoon, J. K. Lee, Y. E. Sung, *Composites, Part B* **2019**, *166*, 613.
[21] J. Liang, L. Zhang, D. XiLi, J. Kang, *Electrochim. Acta* **2020**, *341*, 136030.
[22] J. K. Ling, C. Karuppiah, M. V. Reddy, B. Pal, C. C. Yang, R. Jose, *J. Mater. Res.* **2021**, *36*, 4120.
[23] H. Liu, N. Li, L. Liu, S. Zhang, J. Wang, K. Chang, Y. Du, W. Zhang, *Composites, Part B* **2022**, *243*, 110151.
[24] I. Ostroman, C. Ferrara, S. Marchionna, A. Gentile, N. Vallana, D. Sheptyakov, R. Lorenzi, R. Ruffo, *Small Methods* **2023**, *624*, 2300503.
[25] S. Jolly, S. Husmann, V. Presser, M. Naguib, *J. Am. Ceram. Soc.* **2023**, *106*, 3261.
[26] I. Ostroman, N. Vallana, S. Marchionna, A. Gentile, C. Ferrara, I. C. Pellini, M. Fracchia, N. Pianta, R. Ruffo, *J. Power Sources* **2024**, *624*, 235543.
[27] X. H. Wang, Y. C. Zhou, *J. Mater. Sci. Technol.* **2010**, *26*, 385.
[28] S. Dubois, G. P. Bei, C. Tromas, V. Gauthier-Brunet, P. Gadaud, *Int. J. Appl. Ceram. Technol.* **2010**, *7*, 719.
[29] E. Drouelle, V. Brunet, J. Cormier, P. Villechaise, P. Sallot, F. Naimi, F. Bernard, S. Dubois, *J. Am. Ceram. Soc.* **2020**, *103*, 1270.
[30] G. W. Bentzel, M. Naguib, N. J. Lane, S. C. Vogel, V. Presser, S. Dubois, J. Lu, L. Hultman, M. W. Barsoum, E. N. Caspi, *J. Am. Ceram. Soc.* **2016**, *99*, 2233.
[31] N. J. Lane, S. C. Vogel, E. N. Caspi, S. Dubois, V. Gauthier-Brunet, G. P. Bei, M. W. Barsoum, *J. Am. Ceram. Soc.* **2014**, *97*, 570.
[32] C. Guo, E. Wang, S. Wang, X. Hou, Z. He, T. Liang, K. C. Chou, *Corros. Sci.* **2021**, *180*, 109197.
[33] C. Guo, E. Wang, Y. Liu, Y. Zheng, T. Yang, X. Hou, *Fundam. Res.* **2022**, *2*, 114.
[34] G. M. Song, Y. T. Pei, W. G. Sloof, S. B. Li, J. T. M. De Hosson, S. van der Zwaag, *Scr. Mater.* **2008**, *58*, 13.
[35] T. Brousse, D. Defives, L. Pasquereau, S. M. Lee, U. Herterich, D. M. Schleich, *Ionics* **1997**, *3*, 332.
[36] A. Grant, A. Carroll, Y. Zhang, U. Gulzar, S. A. Ahad, H. Geaney, C. O. Dwyer, *J. Electrochem. Soc.* **2023**, *170*, 120505.
[37] N. Vallana, I. Ostroman, A. Gentile, S. Marchionna, C. Ferrara, D. Sheptyakov, A. Fitch, M. Fracchia, N. Pianta, A. G. Marrani, T. Kim, C. Park, C. Lee, H.-W. Lee, L. Stievano, R. Ruffo, SSRN abstract ID 5072520, https://dx.doi.org/10.2139/ssrn.5072520.
[38] J. Yan, W. Shen, L. Wang, Y. Zhuang, S. Guo, *J. Phys. Chem. C* **2022**, *126*, 14813.
[39] J. Mei, J. Wang, H. Gu, Y. Du, H. Wang, Y. Yamauchi, T. Liao, Z. Sun, Z. Yin, *Adv. Mater.* **2020**, *33*, 2004920.
[40] J. Wang, B. Liu, Z. Wang, Z. Liu, L. Li, M. Wang, X. Meng, Y. Yong, H. Wang, Z. Yin. *Nano Micro Small* **2025**, *21*, 2410380.

Manuscript received: December 28, 2024
Revised manuscript received: March 3, 2025
Version of record online: